Simulation of the global ENSO–Tropical cyclone teleconnection by a high-resolution coupled general circulation model

Simulation of the Global ENSO–Tropical Cyclone Teleconnection by a High-Resolution Coupled General Circulation Model

RAY BELL

Department of Meteorology, University of Reading, Reading, United Kingdom

KEVIN HODGES

NERC Centre for Earth Observation, University of Reading, Reading, United Kingdom

PIER LUIGI VIDALE

National Centre for Atmospheric Science, Department of Meteorology, University of Reading, Reading, United Kingdom

JANE STRACHAN AND MALCOLM ROBERTS

Met Office Hadley Centre, Exeter, United Kingdom

(Manuscript received 6 September 2013, in final form 15 April 2014)

ABSTRACT

This study assesses the influence of the El Niño–Southern Oscillation (ENSO) on global tropical cyclone activity using a 150-yr-long integration with a high-resolution coupled atmosphere–ocean general circulation model [High-Resolution Global Environmental Model (HiGEM); with N144 resolution: ~90 km in the atmosphere and ~40 km in the ocean]. Tropical cyclone activity is compared to an atmosphere-only simulation using the atmospheric component of HiGEM (HiGAM). Observations of tropical cyclones in the International Best Track Archive for Climate Stewardship (IBTrACS) and tropical cyclones identified in the Interim ECMWF Re-Analysis (ERA-Interim) are used to validate the models. Composite anomalies of tropical cyclone activity in El Niño and La Niña years are used. HiGEM is able to capture the shift in tropical cyclone locations to ENSO in the Pacific and Indian Oceans. However, HiGEM does not capture the expected ENSO–tropical cyclone teleconnection in the North Atlantic. HiGAM shows more skill in simulating the global ENSO–tropical cyclone teleconnection; however, variability in the Pacific is overpronounced. HiGAM is able to capture the ENSO–tropical cyclone teleconnection in the North Atlantic more accurately than HiGEM. An investigation into the large-scale environmental conditions, known to influence tropical cyclone activity, is used to further understand the response of tropical cyclone activity to ENSO in the North Atlantic and western North Pacific. The vertical wind shear response over the Caribbean is not captured in HiGEM compared to HiGAM and ERA-Interim. Biases in the mean ascent at 500 hPa in HiGEM remain in HiGAM over the western North Pacific; however, a more realistic low-level vorticity in HiGAM results in a more accurate ENSO–tropical cyclone teleconnection.

1. Introduction

Tropical cyclones can cause substantial loss of life and an improved understanding of storm variability can help inform preparation and response to landfalling events. Natural climate variability of the El Niño–Southern Oscillation (ENSO) has a large influence on global storm variability. This has been long observed: for example, Gray (1984) for the North Atlantic, Chan (1985) for the western North Pacific, and Nicholls (1979) for the Australian region. Because of recent advances in available computing resources, general circulation models (GCMs) can now be run with a high enough resolution to simulate different aspects of tropical cyclone activity (e.g., Zhao et al. 2009; Smith et al. 2010; Murakami et al. 2012; Manganello et al. 2012; Strachan et al. 2013). Long integrations of these GCMs can be used to understand the robust responses of tropical cyclones to the phase of

Corresponding author address: Ray Bell, Department of Meteorology, University of Reading, Reading RG6 6BB, United Kingdom. E-mail: r.bell@reading.ac.uk

DOI: 10.1175/JCLI-D-13-00559.1

ENSO beyond the traditional use of observations, as well as to provide a platform to examine the dynamical and thermodynamical mechanisms.

A review of the physical mechanisms that drive regional changes in tropical cyclone activity associated with ENSO is in Camargo et al. (2007b). One strong driver of global tropical cyclone variability is the response of the atmospheric Walker circulation, which can influence regional dynamic and thermodynamic conditions. A weakening of the Walker circulation during El Niño years leads to an increase in upper-tropospheric westerlies over the North Atlantic, for example, which increases vertical wind shear and suppresses tropical cyclone activity (e.g., Gray and Sheaffer 1991; Goldenberg and Shapiro 1996; Kossin et al. 2010). Shaman et al. (2009) also note the importance of Rossby waves influencing upper-level vorticity over the tropical Atlantic, suppressing tropical cyclogenesis during El Niño years. Camargo et al. (2007b) found relative humidity and vertical wind shear are important for the reduction in genesis seen in the North Atlantic using the genesis potential index (GPI) on the National Centers for Environmental Prediction (NCEP) reanalysis data (Kalnay et al. 1996) from 1950 to 2004.

There is a well-known relationship that during El Niño years genesis locations in the western North Pacific shift east along with the warm tropical Pacific sea surface temperatures (SSTs). This is thought to be connected with an eastward expansion of the monsoon trough and westerlies, which increase low-level vorticity (Wang and Chan 2002). However, Camargo et al. (2007b) argue that a decrease in midlevel humidity near the Asian continent during El Niño years suppresses the activity. The shift of tropical cyclones to the central Pacific during El Niño events also occurs in the southwest Pacific, which is also attributed to an extension of the monsoon trough and equatorial westerlies (Chu 2004). In addition, Chand et al. (2013) recently found that an eastward extension of low vertical wind shear and increased relative humidity and SST explain the enhancement of tropical cyclone numbers during El Niño years in that region. Recent work by Diamond et al. (2013) categorizes the type of ENSO event based on the strength of ocean–atmosphere coupling and its impact on tropical cyclone activity in the southwest Pacific. The impact of different types of El Niño on tropical cyclone activity is increasingly gaining attention (Kim et al. 2009) and will be discussed in a future publication using this model.

While the ENSO–tropical cyclone relationship is reasonably well known within each basin, there has only been one study that investigates the global ENSO–tropical cyclone teleconnection in observations. Camargo et al. (2007b) examined how different environmental factors contribute to the ENSO–tropical cyclone teleconnection using the GPI developed by Emanuel and Nolan (2004). Other GPIs are currently being developed to investigate the relationship in specific basins [e.g., Bruyère et al. (2012) for the North Atlantic] as well as an improved statistical relation of the variables to tropical cyclone genesis (Tippett et al. 2011; McGauley and Nolan 2011).

The ENSO–tropical cyclone teleconnection has also received little attention in GCM studies compared to research on tropical cyclones and climate change. Wu and Lau (1992) were the first to investigate the global ENSO–tropical cyclone teleconnection using a very coarse atmosphere-only GCM (AGCM) with R15 resolution (7.5° × 4.5°). Vitart and Anderson (2001) used a 10-member ensemble AGCM at T42 (2.8° × 2.8°) to investigate the ENSO–tropical cyclone teleconnection in the North Atlantic. Vitart and Anderson (2001) were able to simulate the expected tropical cyclone response with the phase of ENSO due to simulated changes in vertical wind shear. While the ensemble approach is useful, Vitart and Anderson (2001) only investigated one El Niño event and one La Niña event. More recently, Murakami and Wang (2010) showed a 20-km-resolution AGCM was able to capture the broad tropical cyclone response to ENSO in the North Atlantic, although they did not comment on which simulated parameters were important. AGCM experiments are limited by short integration lengths, which makes it difficult to assess the robustness of the simulated ENSO–tropical cyclone teleconnection. In addition, AGCMs are forced with observed SSTs, which have signatures of time-varying radiative forcing including that from aerosols and greenhouse gases. This makes it difficult to isolate the simulated ENSO–tropical cyclone teleconnection from these experiments. Investigating the ENSO–tropical cyclone using AOGCMs has received less attention because of the larger computational costs involved. In addition, the complexity of understanding tropical cyclone genesis and moving processes has limited progress on understanding the ENSO–tropical cyclone teleconnection.

Shaman and Maloney (2012) investigated the ability of phase 3 of the Coupled Model Intercomparison Project (CMIP3) atmosphere–ocean GCMs (AOGCMs) to simulate the expected large-scale environmental conditions associated with ENSO, which are important for tropical cyclones, over the North Atlantic. Shaman and Maloney (2012) found the impacts of ENSO on Caribbean vertical wind shear were the most poorly simulated. However, the GCMs used in Shaman and Maloney (2012) had coarse horizontal resolution (2° × 2°). These coarse-resolution CMIP3 models have an

inaccurate representation of ENSO itself and ENSO-associated teleconnections (Guilyardi et al. 2009). In addition, coarse-resolution models simulate a poor tropical cyclone climatology (Murakami and Sugi 2010). Higher-resolution GCMs have shown to greatly improve the simulation of ENSO variability (e.g., Shaffrey et al. 2009; Delworth et al. 2012), tropical cyclone climatology (e.g., Strachan et al. 2013), and ENSO-associated teleconnections (e.g., Dawson et al. 2013).

Constant present-day forcing experiments with an AOGCM can be used to assess how well a model is able to simulate modes of natural variability and associated teleconnections. Iizuka and Matsuura (2008) use a high-resolution AOGCM with present-day forcing integrated for 100 yr to investigate the simulated ENSO–tropical cyclone teleconnection in the western North Pacific; Iizuka and Matsuura (2009) use it for the North Atlantic. Both studies show the AOGCM is able to capture the expected tropical cyclone response to ENSO. However Iizuka and Matsuura (2008, 2009) fail to discuss if the AOGCM is capturing the tropical cyclone response because of the expected mechanisms. The results in the North Atlantic by Iizuka and Matsuura (2009) show a spurious trend of increasing tropical cyclone frequency throughout the simulation reducing the credibility of their findings. Kim et al. (2013, manuscript submitted to *J. Climate*) show the simulation of the global ENSO–tropical cyclone teleconnection in a present-day experiment using the Geophysical Fluid Dynamics Laboratory Coupled Model 2.5 (GFDL CM2.5); however, they do not comment on the simulated mechanisms, as their paper focuses on climate change results. It is important to investigate this phenomenon in more than one GCM to improve understanding of the simulated ENSO–tropical cyclone teleconnection.

The ability of the High-Resolution Global Environmental Model (HiGEM) to simulate a realistic ENSO in terms of its amplitude, variability, spatial structure, and associated teleconnections is discussed in Shaffrey et al. (2009). HiGEM simulates Niño-3 (5°S–5°N, 90°–150°W) SST anomalies of a similar variability to those observed in the Hadley Centre Sea Ice and Sea Surface Temperature dataset (HadISST), with a standard deviation of 0.89 K compared to a standard deviation of 0.84 K in HadISST. A composite of the eight largest El Niños measured during December–February (DJF) present a spatial pattern and amplitude that are much closer to observations than in lower-resolution versions of the model. However, the ENSO SST anomalies still extend too far into the western tropical Pacific, which is a common failing of most climate models (Guilyardi et al. 2009). HiGEM has some skill in replicating the observed transitions of the Walker circulation: for example, capturing the precipitation response over the Indian Ocean. More recently, Dawson et al. (2013) investigated the ability of HiGEM to capture the expected extratropical teleconnections associated with El Niño. The upper-level vorticity response is captured by HiGEM in the extratropical Pacific, although it is slightly shifted west of observations.

In this study, we make use of a 150-yr-long integration at present-day CO_2 levels using a high-resolution AOGCM, HiGEM, with the aim to investigate the simulated response of global tropical cyclone activity to ENSO. The present-day forcing removes further anthropogenic influence by holding greenhouse gases and aerosols constant and therefore does not take into account a possible anthropogenic influence on a changing ENSO, such as its frequency or strength. An investigation is made where the mechanisms simulated in the AOGCM are compared with observations and reanalysis data. We also examine the ability of the atmospheric component of HiGEM (HiGAM), forced with Atmospheric Model Intercomparison Project 2 (AMIP-II) SSTs, to capture the expected ENSO–tropical cyclone teleconnection.

The paper is structured as follows: Section 2 describes the models, observations, and reanalysis datasets. The impacts of changing tropical cyclone location and frequency to the phase of ENSO are investigated in section 3, along with an investigation of the changing large-scale environmental conditions in section 4. Section 5 discusses the advantages and shortcomings of the simulated ENSO–tropical cyclone teleconnection in HiGEM and HiGAM. The results of the study are summarized in section 6, along with concluding remarks.

2. Data and methodologies

a. Models

This study uses HiGEM, a high-resolution atmosphere–ocean climate model based on the Met Office Hadley Centre Global Environmental Model, version 1 (HadGEM1; Johns et al. 2006; Ringer et al. 2006). The horizontal resolution of the atmospheric component is 0.83° latitude × 1.25° longitude (N144; 90 km at 50°N). The atmosphere has 38 vertical levels extending to over 39 km in height. The ocean component also has a high resolution: 0.3° × 0.3° (40 km at 50°N) with 40 vertical levels. More details about HiGEM and validation of the global mean state and variability can be found in Roberts et al. (2009) and Shaffrey et al. (2009). The present-day tropical cyclone climatology and response of tropical cyclones to idealized climate change in HiGEM was already presented in Bell et al. (2013). The HiGEM control

simulation was completed using present-day radiative forcing for 150 yr. Also explored is the atmospheric component of HiGEM (HiGAM), forced with prescribed monthly SST and sea ice concentration boundary conditions from AMIP-II for 1979–2002 (Taylor et al. 2000). The ability of HiGAM to simulate tropical cyclone activity in terms of seasonal cycle, interannual variability and intensity is discussed in Strachan et al. (2013).

b. Tropical cyclone tracking algorithm

The objective feature tracking methodology is fully described in Bengtsson et al. (2007) and Strachan et al. (2013). For initial identification and tracking, 850-hPa relative vorticity is computed at a spectral resolution of T42. The initial identification is made for vorticity maxima with intensities greater than $0.5 \times 10^{-5}\,s^{-1}$ in the Northern Hemisphere (minima less than $-0.5 \times 10^{-5}\,s^{-1}$ in the Southern Hemisphere). Systems with a lifetime of over 2 days are retained for further analysis. The tropical cyclone features are identified using intensity thresholds and evidence of a warm core. Track density statistics are used to investigate the spatial distribution of tropical cyclones via the tracking algorithm. Tropical cyclones from the analysis period are composited, and monthly mean storm transits per unit area (equivalent to a 5° spherical cap: approximately $10^6\,km^2$) are calculated.

c. Observational and reanalysis data

Global observed tropical cyclones are obtained from the International Best Track Archive for Climate Stewardship (IBTrACS; Knapp et al. 2010) for the 1979–2010 period. Observed SSTs from the HadISST for the 1979–2010 period, which has a resolution of 1° × 1° (Rayner et al. 2003), are used for validation of the coupled model. HadISST is composed of in situ sea surface observations and satellite-derived estimates at the sea surface. The period of 1979 onward uses homogeneous data, which have global coverage. Observed precipitation data are obtained from the Global Precipitation Climatology Project (GPCP) dataset for 1979–2010, to investigate the ENSO teleconnection in comparison to the models. GPCP is a 2.5° × 2.5° gridded dataset that combines satellite estimates and rain gauge data (Adler et al. 2003). Precipitation rates in GPCP are produced through combining empirical infrared estimates from geostationary satellites with empirical microwave estimates from polar orbiting satellites. The estimates are adjusted where gauge data are available; however, there are known limitations over the ocean (Smith et al. 2006). Large-scale environmental parameters from the Interim European Centre for Medium-Range Weather Forecasts Re-Analysis (ERA-Interim) are used for 1979–2010 (Dee et al. 2011).

d. Construction of ENSO composites

ENSO events are defined using the normalized Niño-3.4 SST anomalies (in the area 5°S–5°N, 120°–170°W) which had an amplitude of greater than 1 or less than −1 for the DJF period. Tropical cyclone seasons in the Northern Hemisphere (May–November) are defined prior to an ENSO event. The normalized Niño-3.4 SST anomalies during the peak of the Northern Hemisphere tropical cyclone season, August–October (ASO), has a correlation of 0.9 (Pearson correlation) with the normalized Niño-3.4 DJF SST anomalies. Southern Hemisphere tropical cyclone seasons (October–May) were selected during the ENSO event. The seven El Niño events of 1982/83, 1986/87, 1991/92, 1994/95, 1997/98, 2002/03, and 2009/10 and the six La Niña events of 1984/85, 1988/89, 1998/99, 1999/2000, 2007/08, and 2010/11 are composited and compared with the 1979–2010 observed climatology. The ENSO events match those of the National Oceanic and Atmospheric Administration (NOAA) oceanic Niño index (ONI); however, the ONI includes other weaker years as it uses a classification of ±0.5°C [from extended reconstructed SST, version 3b (ERSST.v3b) anomalies in the Niño-3.4 region] for a minimum of five consecutive overlapping seasons. The multivariate ENSO index (MEI; Wolter and Timlin 2011) similarly identifies all the ENSO events, except for the La Niña event of 1984/85. The ENSO events within the time period 1979–2002 are composited in the AGCM HiGAM dataset and compared to its climatology. The AOGCM 150-yr integration of HiGEM simulates 31 El Niño and 25 La Niña events, which are compared with the 150-yr climatology. Composites are used to increase robustness of the ENSO–tropical cyclone teleconnection.

3. Global tropical cyclone activity response to ENSO

The results in this section focus on the simulated response of global tropical cyclone activity during El Niño and La Niña years. The differences in tropical cyclone location and frequency are shown for both HiGAM and HiGEM, with comparisons to tropical cyclones observed in IBTrACS and those identified in ERA-Interim.

a. ENSO and tropical cyclone location

Tropical cyclone track densities of El Niño and La Niña years minus the climatology are shown in Fig. 1. The tropical cyclone location changes in IBTrACS show an increase in tropical cyclones toward the date line in

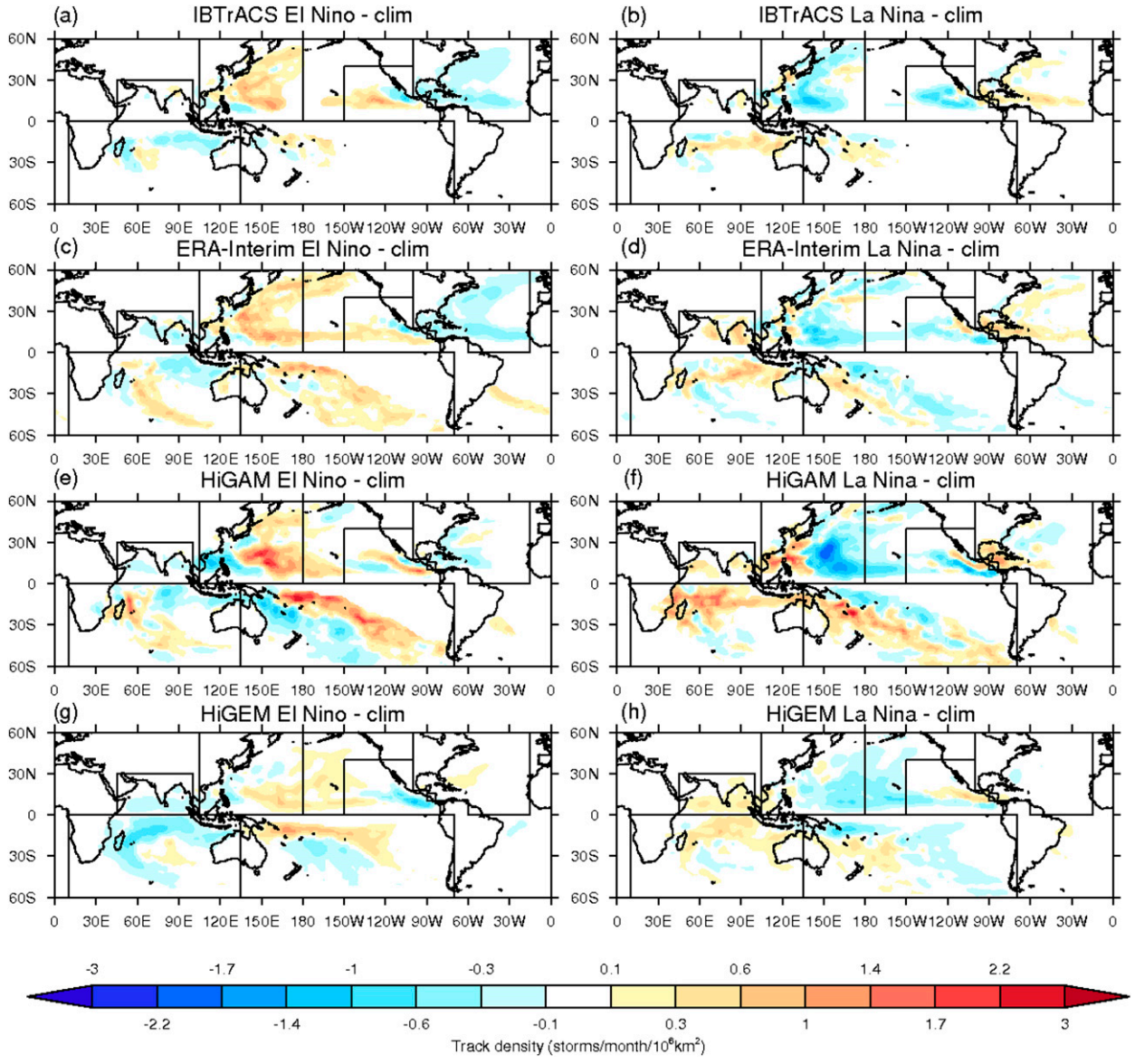

FIG. 1. Tropical cyclone track density (storm transits/month/10^6 km^2 or equivalent to a 5° radius) during May–November in the Northern Hemisphere and October–May in the Southern Hemisphere: for IBTrACS (a) El Niño years minus 1979–2010 climatology and (b) La Niña years minus 1979–2010 climatology; for ERA-Interim (c) El Niño years minus 1979–2010 climatology and (d) La Niña years minus 1979–2010 climatology; for HiGAM (e) El Niño years minus 1979–2002 climatology and (f) La Niña years minus 1979–2002 climatology; and for HiGEM (g) El Niño years minus 150-yr climatology and (h) La Niña years minus 150-yr climatology.

the western North Pacific, as found in Wang and Chan (2002) and Camargo et al. (2007b). Tropical cyclones are suppressed in the North Atlantic during El Niño years and enhanced during La Niña years, a well-known response (Gray and Sheaffer 1991; Goldenberg and Shapiro 1996; Kossin et al. 2010). The increase in tropical cyclone activity in the Bay of Bengal during La Niña year has also been found by Felton et al. (2013). In the Southern Hemisphere, there is a reduction of tropical cyclones to the west of Australia during El Niño events. The opposite is true for La Niña events. Tropical cyclones form closer to the east coast of Australia in the South Pacific during El Niño years and farther offshore during La Niña years, which is discussed in Kuleshov et al. (2008).

There are some differences of tropical cyclone location changes in IBTrACS from those tracked in ERA-Interim. This is in part due to the tracking algorithm applied to ERA-Interim, as we track storms from their genesis to lysis via T42 vorticity, whereas IBTrACS is

based on observations of near-surface sustained wind speed (see Strachan et al. 2013). However, when focusing on the tropics it can be seen that that the tropical cyclones tracked in ERA-Interim match very closely to those in IBTrACS. This provides increased confidence in the tracking algorithm used. The tropical cyclone location changes in ERA-Interim obtained by using an explicit tracking algorithm are similar to the GPI changes in Camargo et al. (2007b). However, the large reduction of tropical cyclone activity in the North Atlantic during El Niño years, which is similar to observations, does not correspond with the change in GPI shown in Camargo et al. (2007b). Similarly, Murakami and Wang (2010) found simulated tropical cyclone changes with ENSO did not correspond to GPI changes in this basin.

HiGAM captures the response of tropical cyclone location to ENSO in the Pacific and Indian Oceans. In the North Atlantic, variability is confined to the Caribbean because of biases in the tropical cyclone climatology (Strachan et al. 2013; Bell et al. 2013). The variability is over pronounced in the western North Pacific in HiGAM compared with observations and ERA-Interim.

HiGEM is able to capture broadly the shift in tropical cyclones in the Pacific and Indian Oceans. However, the tropical cyclones show a shift in location which is more meridional as opposed to the zonal shift in observations in the South Pacific. This is likely to be related to the meridional shift of ENSO-associated precipitation in HiGEM (see Fig. 20. of Shaffrey et al. 2009). HiGEM is unable to capture the expected response of tropical cyclone location changes in the North Atlantic, with a small tendency to simulate more tropical cyclones during El Niño years, the opposite of observations. There are known biases of tropical cyclones in the mean state in this basin (Bell et al. 2013), which likely limit the expected ENSO variability being captured and are discussed later. However, this limitation is not present in all AOGCMs. The Geophysical Fluid Dynamics Laboratory Coupled Model, version 2.5 (GFDL CM2.5; Delworth et al. 2012), which has an atmospheric resolution of 50 km, captures the expected sign of the tropical cyclone response to ENSO in the North Atlantic, even though the model similarly simulates a smaller tropical cyclone climatology than observed (Kim et al. 2013, manuscript submitted to *J. Climate*). The higher atmospheric resolution is likely to be key in capturing this, just as Strachan et al. (2013) found atmospheric resolution to be important for a better representation of interannual variability in the North Atlantic, which mainly came from the improvement in interannual variability of vertical wind shear. In addition, Murakami and Wang (2010) were able to capture the ENSO–tropical cyclone teleconnection in the North Atlantic using an AGCM with 20-km resolution.

b. *ENSO and tropical cyclone frequency*

The effect of ENSO on tropical cyclone counts in each basin is shown in Fig. 2. The average number of tropical cyclones that form in each basin is given in the text below the percentage change. The North Atlantic shows the greatest response of tropical cyclone frequency with ENSO. Tropical cyclones are less frequent in El Niño years by 35% and more frequent in La Niña years by 18%. Klotzbach (2011) found a more symmetrical response of tropical cyclone numbers in El Niño and La Niña years using a longer time period of 1900–2009. However, there are uncertainties in the historical tropical cyclone record (Landsea and Franklin 2013) and historical tropical Pacific SSTs (Solomon and Newman 2012), especially in the early twentieth century. Slightly more tropical cyclones form in El Niño years than in La Niña years in the western North Pacific (Chan and Liu 2004). There is no change in the observed number of tropical cyclones that form each year in the north Indian basin with ENSO.

There are some notable differences between tropical cyclone frequency changes in ERA-Interim and IBTrACS. The variability of tropical cyclones in response to ENSO is much more pronounced in ERA-Interim compared with IBTrACS in the north Indian Ocean. Tropical cyclones are 18% less frequent during La Niña years in the north Indian Ocean in ERA-Interim, whereas in IBTrACS there is no change in the number of tropical cyclones in El Niño or La Niña years. However, the observations in the north Indian Ocean have a large uncertainty shown by the confidence intervals. It should be noted that the tracking algorithm may pick up monsoon depressions in this region similar to other tracking algorithms. ERA-Interim shows a greater percentage variability of tropical cyclones in response to ENSO in the North Atlantic and western North Pacific compared with IBTrACS.

HiGAM simulates a much stronger response of tropical cyclone frequency to ENSO in the north Indian Ocean than observed. However, the response is associated with large uncertainty due to the limited sample size of ENSO events. HiGAM is also able to capture the expected response in the North Atlantic, although the interannual variability is large shown by the confidence intervals. HiGAM does not simulate the observed magnitude of change of tropical cyclone frequency in the North Atlantic, with a 10% reduction in the number

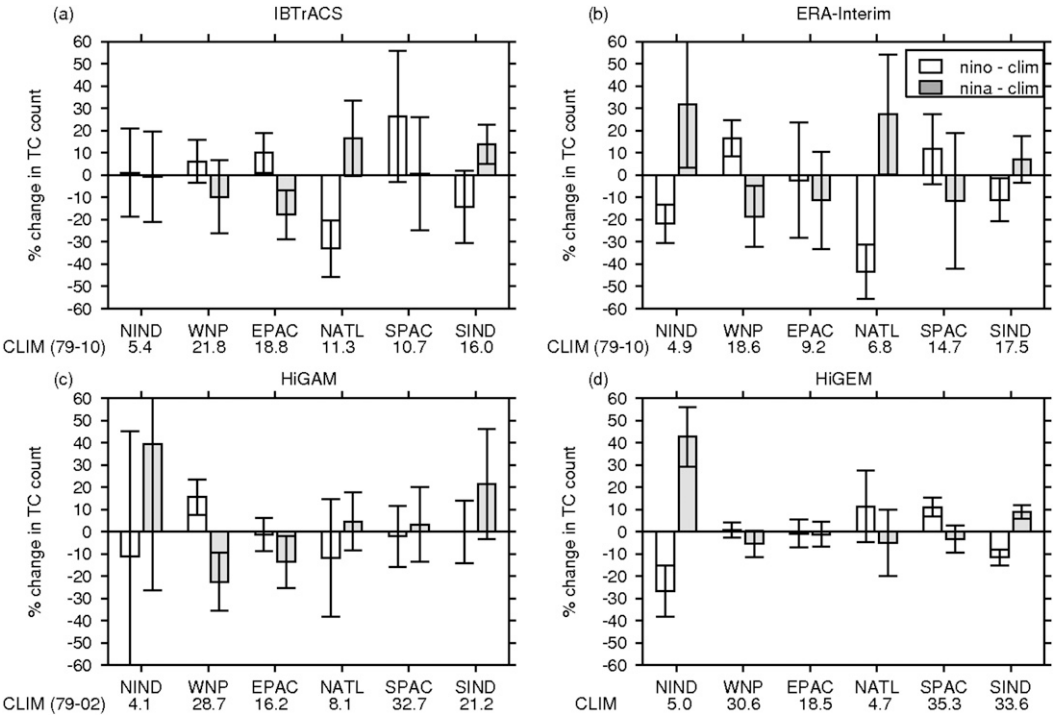

FIG. 2. Percentage change of tropical cyclone counts in El Niño years and La Niña years compared to climatology: (a) IBTrACS (1979–2010), (b) ERA-Interim (1979–2010), (c) HiGAM (1979–2002), and (d) HiGEM. The climatology is shown at the bottom of the *x*-axis label. Error bars denote the 90% confidence interval.

of tropical cyclones that form compared to a 35% reduction shown by IBTrACS during El Niño years.

The tropical cyclone frequency response in the south Indian Ocean is smaller in HiGEM than in HiGAM and therefore simulates a response similar to that observed. Although HiGEM captures the shift of tropical cyclones in the Pacific region to the phase of ENSO, the amplitude of the tropical cyclone frequency changes is much less than observed. One outstanding difference between HiGEM and HiGAM is that HiGEM simulates the response of tropical cyclone frequency change in the North Atlantic with ENSO of the opposite sign to HiGAM and that expected, although HiGAM simulates large variability in the number of tropical cyclones per season during El Niño and La Niña years shown by the large confidence intervals.

4. ENSO and large-scale environmental conditions

The number of tropical cyclones which form each year and in each basin depends largely on the large-scale environment (Camargo et al. 2007a,b). The results in this section investigate the changing large-scale environmental conditions associated with ENSO. Variables considered include SST, precipitation, vertical wind shear, vorticity, and tropical circulation.

a. Sea surface temperature

Figure 3 shows the change in SST during July–October (JASO), the peak of the Northern Hemisphere tropical cyclone season, for El Niño and La Niña years compared to the climatology of HadISST, AMIP-II SST, and HiGEM. The warmest SST associated with ENSO during JASO can be seen to extend too far into the western tropical Pacific in HiGEM. In addition, the meridional extent of the ENSO-associated SST is wider in HiGEM than in HadISST, which is associated with biases in the simulated atmospheric response. This may be responsible for the large response of tropical cyclones in the central Pacific to ENSO, which is not present in observations or ERA-Interim seen in Fig. 1. However, the results from HiGAM indicate poor simulated spatial patterns of SST variability do not explain all of HiGEM's deficiencies at simulating the expected ENSO–tropical cyclone teleconnections.

b. Precipitation

The precipitation response to ENSO is a good indicator of the atmospheric teleconnections in the tropics (Alexander et al. 2002). Examining the accuracy of simulated ENSO-associated precipitation provides a test bed for comparison of modeled to observed

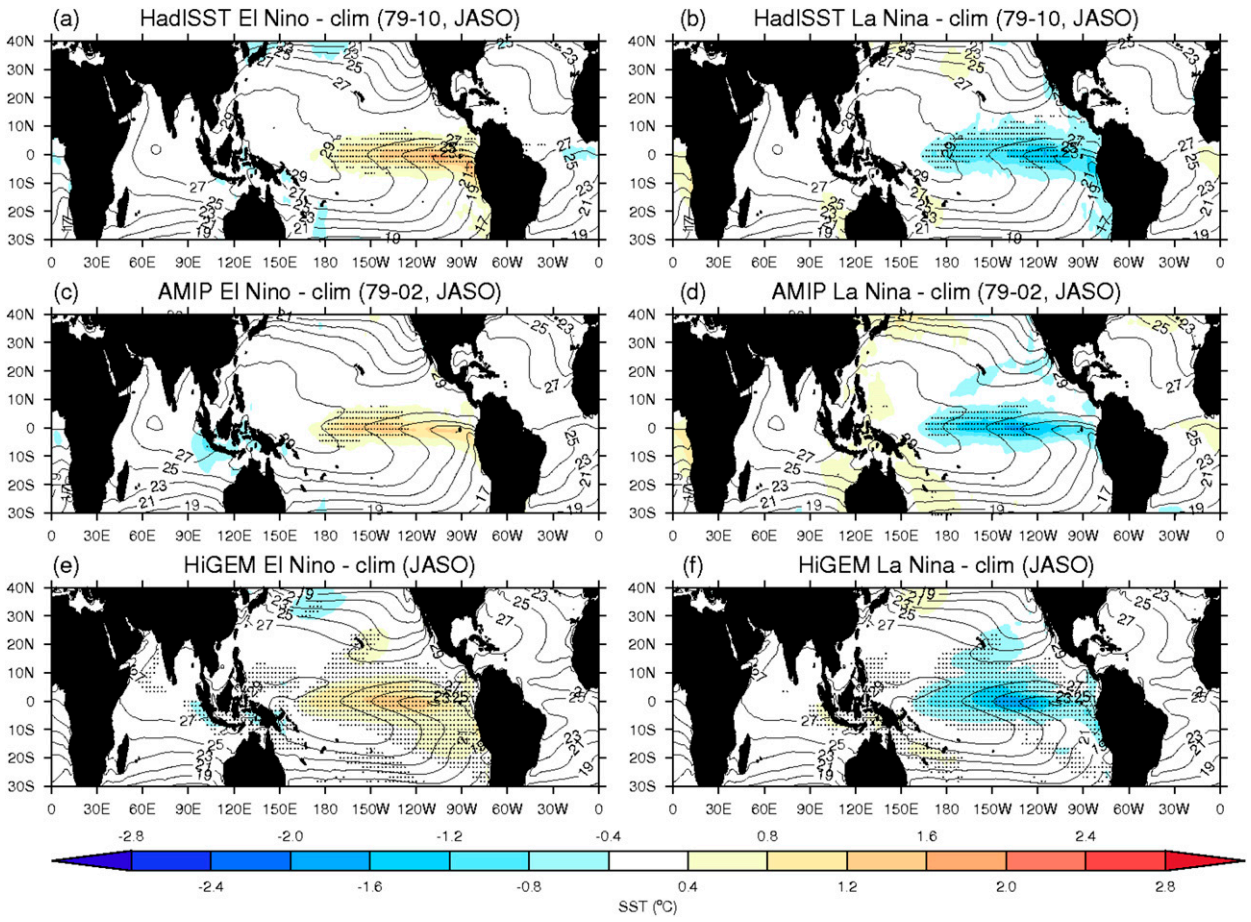

FIG. 3. Sea surface temperature (°C), July–October for (a) HadISST El Niño years minus 1979–2010 climatology, (b) HadISST La Niña years minus 1979–2010 climatology, (c) AMIP SST El Niño years minus 1979–2002 climatology, (d) AMIP La Niña years minus 1979–2002 climatology (e) HiGEM El Niño years minus 150-yr climatology, and (f) HiGEM La Niña years minus 150-yr climatology. The climatology is shown in black contours for HadISST in (a),(b); for AMIP SST in (c),(d); and for HiGEM in (e),(f). Stippling shows where changes have a p value <0.0001 using a Student's t test.

precipitation (Langenbrunner and Neelin 2013). Figure 4 shows JASO precipitation changes in El Niño and La Niña years compared to the climatology for GPCP, HiGAM, and HiGEM. The climatology for each dataset is shown in black contours. Tropical cyclone activity follows large-scale changes in precipitation with ENSO (shown in Fig. 1). HiGAM is able to simulate the expected precipitation response across the tropics; however, the magnitude of the response is larger in HiGAM than seen in GPCP. HiGEM captures the shift of precipitation into the central Pacific and the suppression of precipitation around the Maritime Continent during El Niño years. However, the ENSO–precipitation response is too strong in HiGEM over the Indian Ocean, as noted by Shaffrey et al. (2009). During El Niño years, GPCP shows that precipitation is suppressed over the Caribbean and enhanced during La Niña years. While HiGAM captures this variability, HiGEM simulates no variability. The lack of precipitation in the mean state of HiGEM in the Caribbean also contributes to the poor simulation of the teleconnection (see Fig. 6; Shaffrey et al. 2009).

c. *Walker circulation*

The Walker circulation response to ENSO acts as an ''atmospheric bridge'' (Alexander et al. 2002) for tropical cyclone activity to respond in basins away from the Pacific. Figure 5 shows the Walker circulation for El Niño and La Niña years compared to climatology in ERA-Interim, HiGAM, and HiGEM. The Walker circulation influences regions of large-scale motion as well as shifts the location of vertical wind shear patterns, which modulate tropical activity (Kossin et al. 2010). The anomalously warm SSTs in the central Pacific during El Niño years favors convection, which drives the large-scale tropical atmospheric circulation. The descending

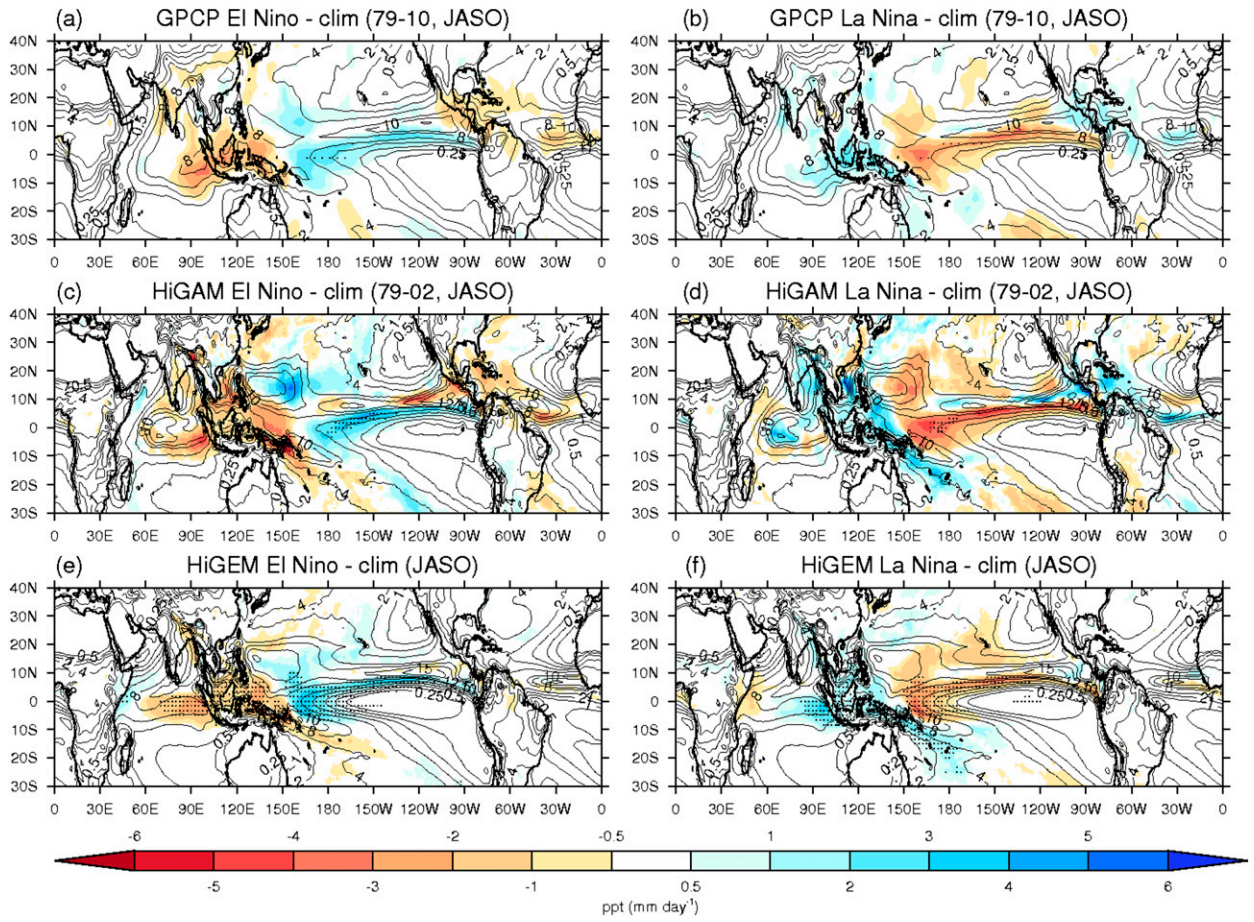

FIG. 4. Precipitation (mm day^{-1}), July–October for (a) GPCP El Niño years minus 1979–2010 climatology, (b) GPCP La Niña years minus 1979–2010 climatology, (c) HiGEM El Niño years minus 1979–2002 climatology, (d) HiGAM La Niña years minus 1979–2002 climatology, (e) HiGEM El Niño years minus 150-yr climatology, and (f) HiGEM La Niña years minus 150-yr climatology. The climatology is shown in black contours for GPCP in (a),(b); HiGAM in (c),(d); and HiGEM in (e),(f). Stippling shows where changes have a p value <0.0001 using a Student's t test.

motion over the Indian Ocean, at around 90°E, is too strong in both HiGAM and HiGEM, leading to greater ENSO–tropical cyclone variability. The region of maximum ascent during El Niño years in the central Pacific is constrained to around 160°E in HiGEM, whereas in ERA-Interim the region of maximum ascent occurs over a broad region from 160° to 190°E. Similarly, during the La Niña phase, HiGEM shows enhanced subsidence throughout the central Pacific east of 180°E, which was not found in ERA-Interim. HiGEM does not show the change in vertical motion over the North Atlantic seen in HiGAM and ERA-Interim, explaining the erroneous response of tropical cyclones in this region. A change in the upper-level circulation can be seen in ERA-Interim around 280°E, which may influence the mean vertical motion over the North Atlantic. This driving mechanism is not simulated and as a result HiGEM does not capture the expected ENSO–tropical cyclone variability in the North Atlantic. The change in both vertical motion and upper-level circulation in the North Atlantic is somewhat better simulated in HiGEM during La Niña years compared to El Niño years; however, the observed response is smaller in La Niña years than El Niño years. The lack of ENSO–SST variability in the tropical east Pacific in HiGEM may impact the Hadley cell (Wang 2002), which may also relate to the poor simulation of ENSO-associated vertical wind shear over the northeast Pacific and North Atlantic. The localized ascending motion around 160°E during an El Niño event in HiGEM may prevent the upper-tropospheric circulation response over the North Atlantic.

d. *Vertical wind shear*

Vertical wind shear is defined as the magnitude of the vector difference between winds at 850 and 200 hPa. The

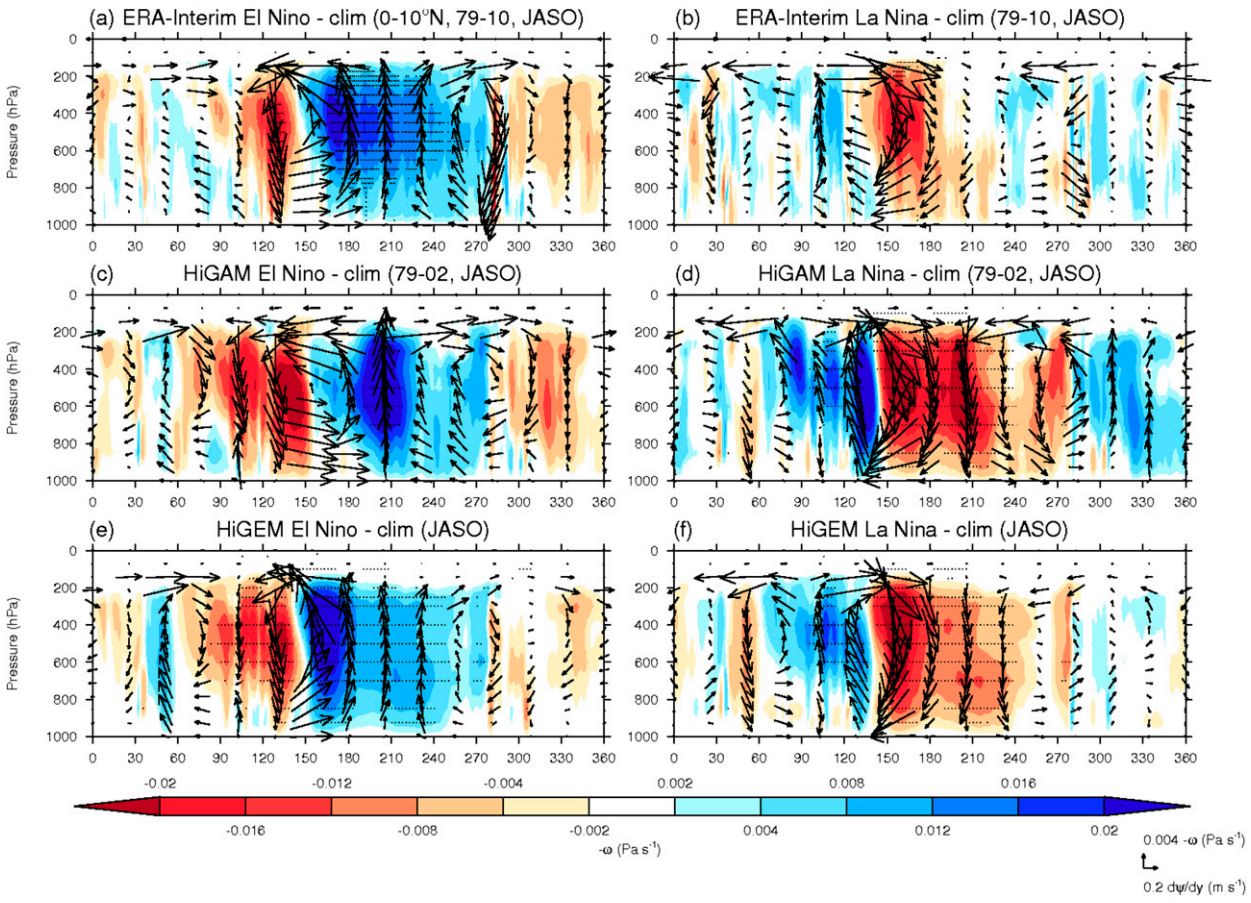

FIG. 5. Height–longitude cross section of Walker circulation, 0°–10°N, for July–October for (a) ERA-Interim El Niño years minus 1979–2010 climatology, (b) ERA-Interim La Niña years minus 1979–2010 climatology, (c) HiGEM El Niño years minus 1979–2002 climatology, (d) HiGAM La Niña years minus 1979–2002 climatology, (e) HiGEM El Niño years minus 150-yr climatology, and (f) HiGEM La Niña years minus 150-yr climatology. The colors show mean ascent ($-\omega$) and the vectors are mean ascent and a change in the velocity potential with respect to longitude. Stippling shows where changes have a p value <0.0001 using a Student's t test.

response of vertical wind shear to ENSO during JASO is shown in Fig. 6. HiGAM is able to capture the shift in vertical wind shear in El Niño and La Niña years when compared to ERA-Interim, although the simulated response is stronger in magnitude. Vertical wind shear is also much stronger in HiGAM than in HiGEM. Figure 3 shows AMIP-II-associated ENSO SSTs are constrained along the equator more so than in HadISST and HiGEM. The larger meridional SST gradient will result in stronger upper-level westerlies via thermal wind balance which will increase vertical wind shear. In addition, as the atmosphere in HiGAM has a larger source of heat without the presence of air–sea coupled feedbacks, the large-scale ENSO-associated tropical convection is more intense and therefore drives stronger winds. The responses observed in the west Pacific and Indian Oceans are captured well by HiGEM, although with a slightly reduced magnitude than that seen in ERA-Interim. The smaller magnitude response over the western North Pacific can help to explain why tropical cyclones show less variability in HiGEM than observed. ERA-Interim reveals a dipole of vertical wind shear over the northeast Pacific and North Atlantic due to the response of ENSO, which was also noted by Aiyyer and Thorncroft (2006). This pattern explains the dipole of tropical cyclone activity between the North Atlantic and northeast Pacific (Frank and Young 2007; Maue 2009). Camargo et al. (2007b) also note that vertical wind shear is an important parameter for explaining the ENSO–tropical cyclone teleconnection in these basins. HiGEM does not capture the expected vertical wind shear shift in this region.

e. *Low-level vorticity*

Low-level vorticity represents the ''spin'' of the atmosphere that is required to form cyclonically rotating

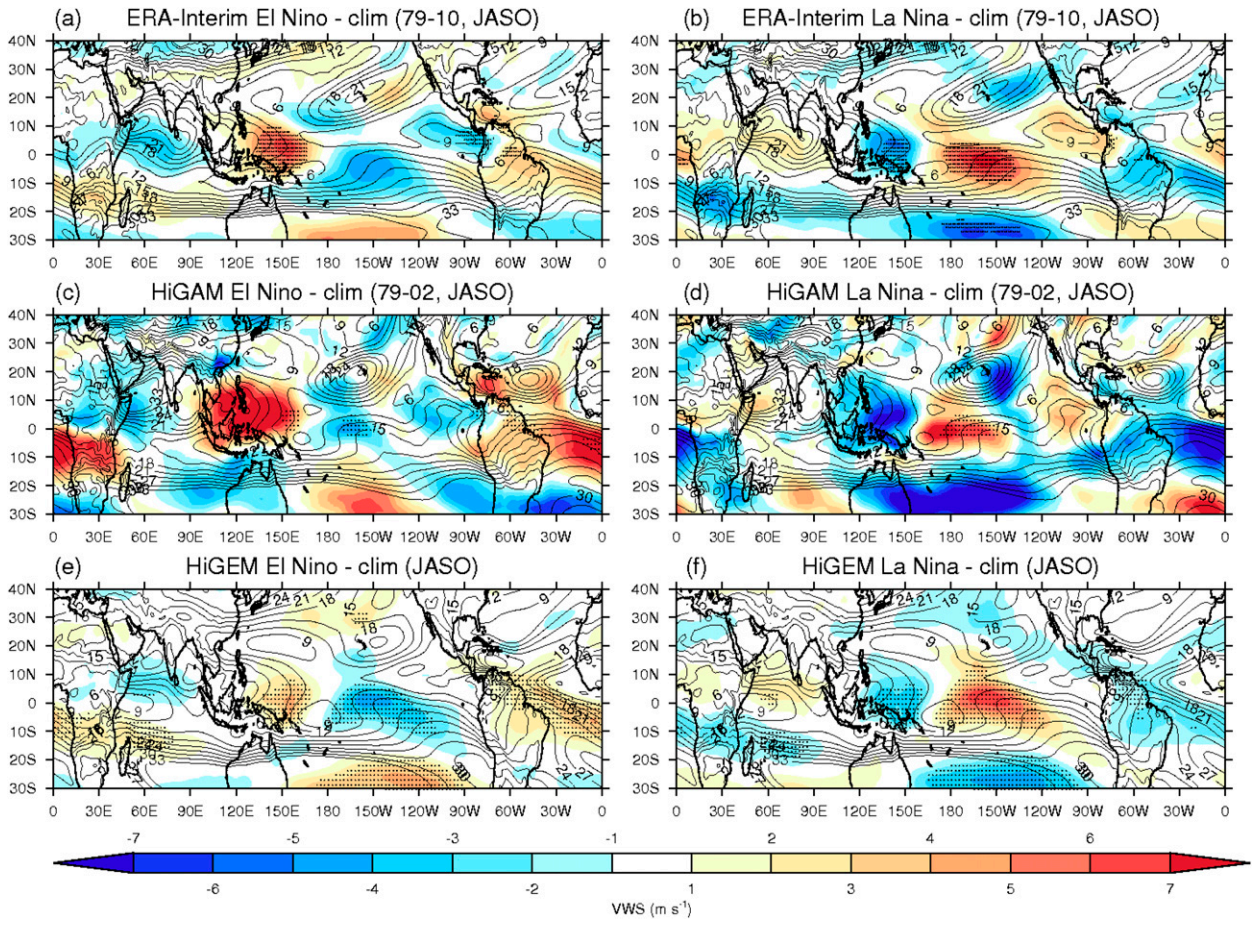

FIG. 6. Vertical wind shear ($m\,s^{-1}$) for July–October for (a) ERA-Interim El Niño years minus 1979–2010 climatology, (b) ERA-Interim La Niña years minus 1979–2010 climatology, (c) HiGEM El Niño years minus 1979–2002 climatology, (d) HiGAM La Niña years minus 1979–2002 climatology, (e) HiGEM El Niño years minus 150-yr climatology, and (f) HiGEM La Niña years minus 150-yr climatology. The climatology is shown in black contours for ERA-Interim in (a),(b); HiGAM in (c),(d); and HiGEM in (e),(f). Stippling shows where changes have a p value <0.0001 using a Student's t test.

storms. Camargo et al. (2007b) note that low-level vorticity is important for tropical cyclogenesis with ENSO in the western North Pacific. Figure 7 shows the 850-hPa JASO relative vorticity for El Niño and La Niña years compared to climatology in ERA-Interim, HiGAM, and HiGEM. The observed vorticity changes in the western North Pacific match those of Wang and Chan (2002) and Mori et al. (2013). HiGAM simulates an increase in vorticity north of the equator in the Pacific with a similar magnitude than that observed in ERA-Interim during El Niño years. There is a large change in vorticity in the western North Pacific around 20°N, 150°E in HiGAM during El Niño and La Niña events that is stronger than observed. HiGAM is able to simulate the large-scale observed response of vorticity over the tropical northeast Pacific and North Atlantic. HiGEM broadly captures the increase in vorticity in the Pacific region during El Niño years, albeit weaker than observed. In addition, the decrease in vorticity in the main development in the north Indian Ocean during El Niño years is simulated in HiGEM. The vorticity response during La Niña years is poorly simulated to the west of Hawaii. Iizuka and Matsuura (2008) similarly found that vorticity does not decrease as much as in observations during La Niña years in the eastern parts of the western North Pacific. HiGEM simulates no change in relative vorticity in the tropical northeast Pacific and North Atlantic.

f. *Upper-level circulation*

The upper-level circulation response to ENSO is investigated further using the velocity potential, an integrated measurement of the irrotational part of the upper-level flow, and the streamfunction, the rotational part. The streamfunction highlights the anomalous wave propagation, whereas the velocity potential highlights the forcing of these waves. Figure 8 shows the velocity

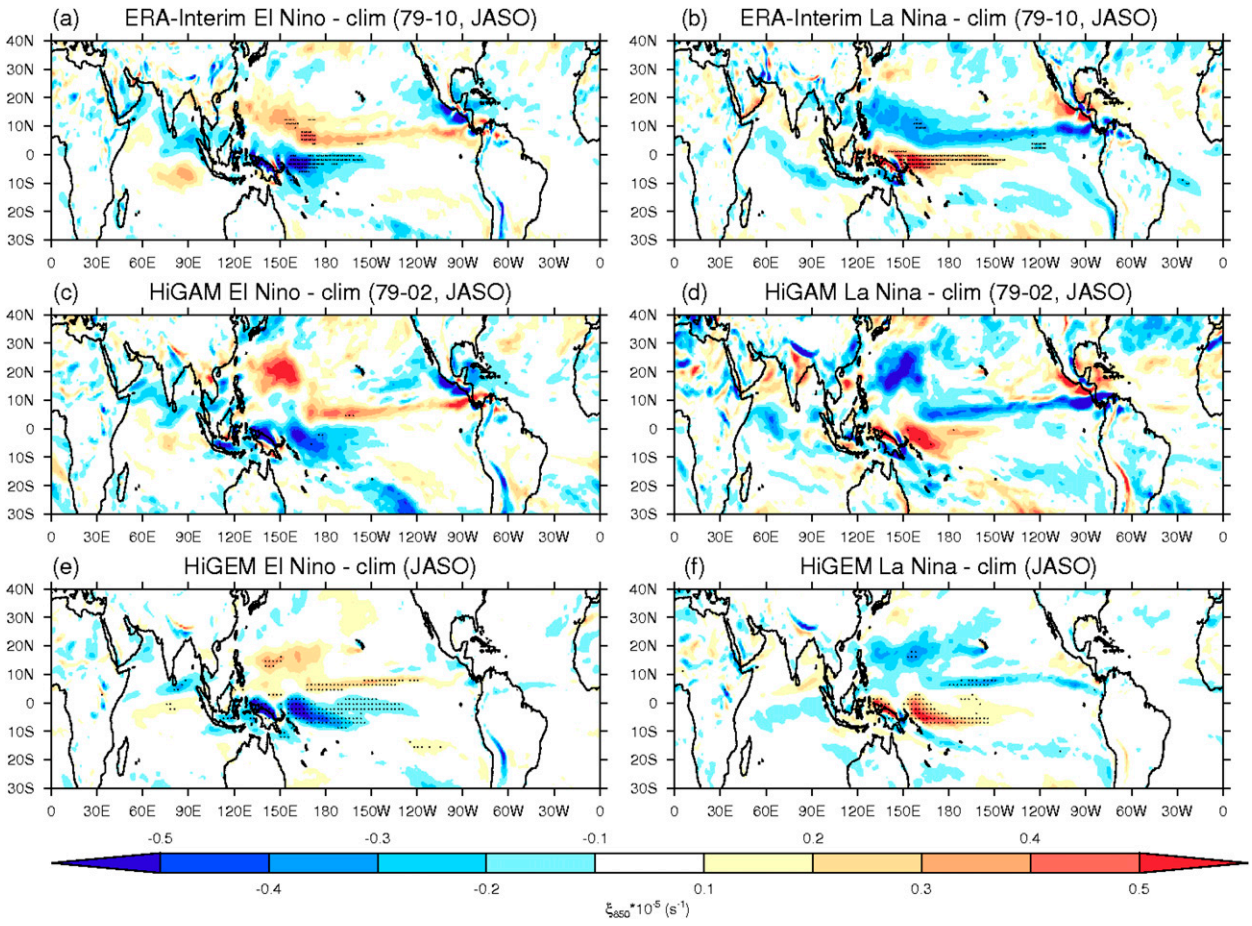

FIG. 7. The 850-hPa relative vorticity ($1 \times 10^{-5}\,s^{-1}$) for July–October for (a) ERA-Interim El Niño years minus 1979–2010 climatology, (b) ERA-Interim La Niña years minus 1979–2010 climatology, (c) HiGEM El Niño years minus 1979–2002 climatology, (d) HiGAM La Niña years minus 1979–2002 climatology, (e) HiGEM El Niño years minus 150-yr climatology, and (f) HiGEM La Niña years minus 150-yr climatology. Stippling shows where changes have a p value <0.0001 using a Student's t test.

potential and streamfunction at 200 hPa during JASO for ERA-Interim, HiGAM, and HiGEM. ERA-Interim shows that in El Niño years twin anticyclones straddle the equator as a response to increased convection in the central Pacific (Spencer and Slingo 2003), similar to a Gill-type response (Gill 1980). In ERA-Interim and HiGAM during El Niño years, the upper-level divergent circulation is constrained to the central Pacific, which was also found in the ECHAM5 model by Bengtsson et al. (2007). HiGEM simulates enhanced upper-level convergence in the Indian Ocean, which also explains the greater tropical cyclone variability related to anomalous large-scale ascent. The spatial extent of the upper-level divergent circulation in HiGEM reaches too far into the North Atlantic from the central Pacific. As a result of the spatial errors in the maximum velocity potential in HiGEM, the upper-level wave propagation is not captured over the North Atlantic, which has previously been related to tropical cyclogenesis (Shaman et al. 2009).

g. *Thermodynamic versus dynamic influences*

Figures 9 and 10 show the relationships between large-scale environmental conditions that are important for tropical cyclone activity over the main development regions and tropical cyclone counts for the North Atlantic and western North Pacific, respectively. The area average used for the North Atlantic is the same as in Bell et al. (2013): 10°–20°N, 275°–340°E. The region with the largest change in tropical cyclone activity is used for the western North Pacific: 5°–20°N, 130°–170°E. This analysis includes the following: thermodynamic variables of SST and relative humidity at 700 hPa, dynamic variables of relative vorticity at 850 hPa, mean ascent at 500 hPa ($-\omega_{500}$), and vertical wind shear. The figures highlight biases in the mean state of the models as well as limitations in

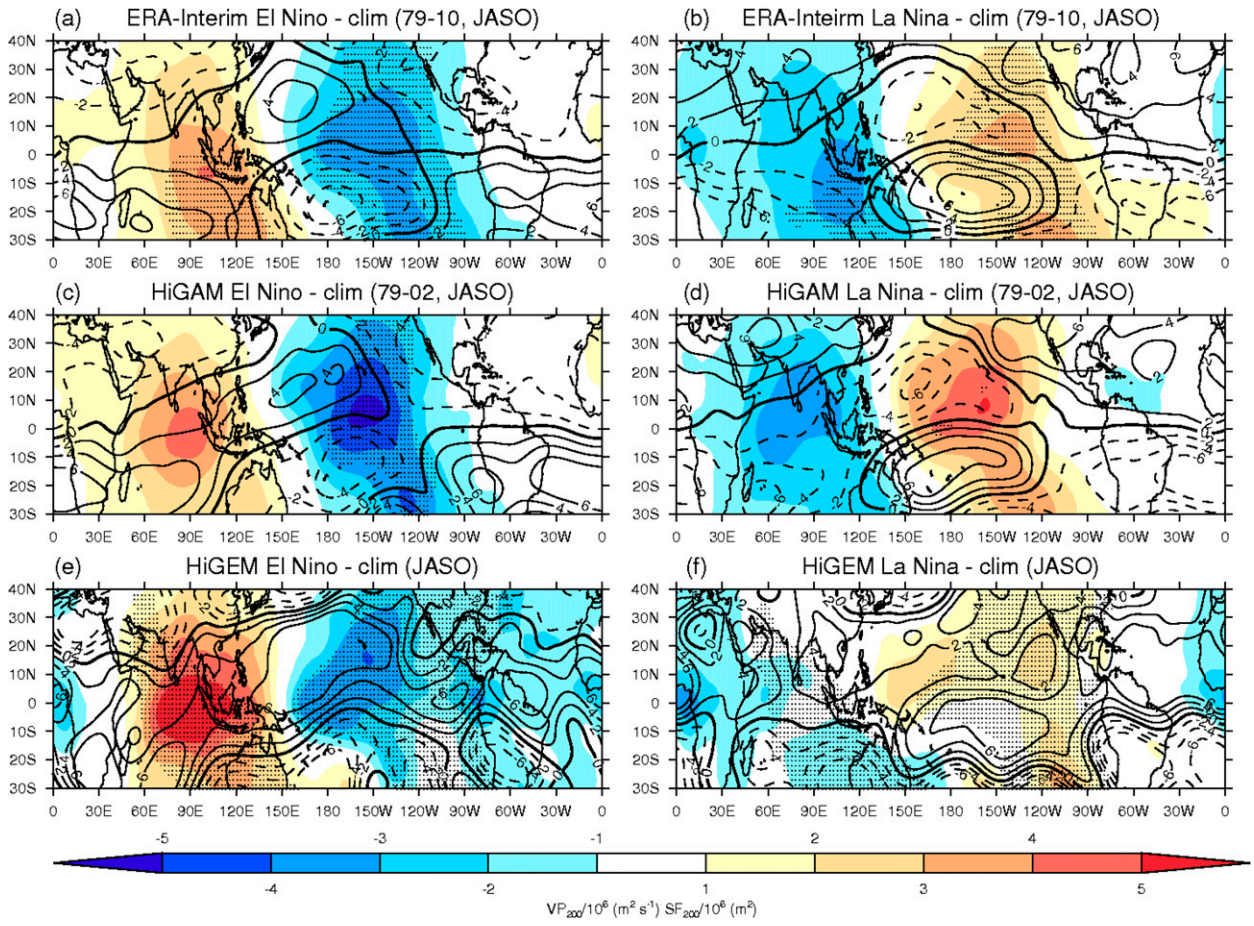

FIG. 8. The 200-hPa velocity potential ($1 \times 10^{-6}\,m^2\,s^{-1}$) in colors and the 200-hPa streamfunction ($1 \times 10^{-6}\,m^2$) in black contours for July–October for (a) ERA-Interim El Niño years minus 1979–2010 climatology, (b) ERA-Interim La Niña years minus 1979–2010 climatology, (c) HiGAM El Niño years minus 1979–2002 climatology, (d) HiGAM La Niña years minus 1979–2002 climatology, (e) HiGEM El Niño years minus 150-yr climatology, and (f) HiGEM La Niña years minus 150-yr climatology. Stippling shows where changes have a p value <0.0001 using a Student's t test.

capturing the magnitude of ENSO-associated large-scale environmental changes. Figures 9a and 10a show Niño-3.4 SSTs. It can be seen that HiGEM has a cool SST bias in the tropical Pacific, although it captures the expected magnitude of ENSO SST anomalies.

In the North Atlantic, it can be seen that vertical wind shear is an important parameter for tropical cyclone activity in ERA-Interim, which is also discussed in Camargo et al. (2007b). The mean vertical wind shear is too strong in HiGAM and more so in HiGEM, which explains the reduced mean number of tropical cyclones compared to observations. This was also found in other GCMs (Shaman and Maloney 2012). The associated change of vertical wind shear with ENSO in HiGEM is opposite to that observed, with stronger vertical wind shear during El Niño years and slightly more tropical cyclones. The coupled model used in Iizuka and Matsuura (2009) was able to simulate the vertical wind shear response, although the simulated amplitude of the Niño-3.4 SST anomalies are much larger than observed. Tropical cyclones are not suppressed as strongly during El Niño in HiGAM compared to ERA-Interim, as the change in large-scale deep ascent is not captured. Although vertical wind shear shows a slight increase in La Niña years in HiGAM, the number of tropical cyclones increases because of an increase in midlevel relative humidity and mean ascent at 500 hPa. The thermodynamic parameters are of secondary importance to dynamic parameters in explaining the tropical cyclone response in the North Atlantic in HiGAM. HiGEM simulates both a poor mean state and little variability of midlevel relative humidity and mean ascent at 500 hPa and therefore does not capture the expected ENSO–tropical cyclone teleconnection.

In the western North Pacific, HiGAM and HiGEM simulate too many tropical cyclones, which is discussed

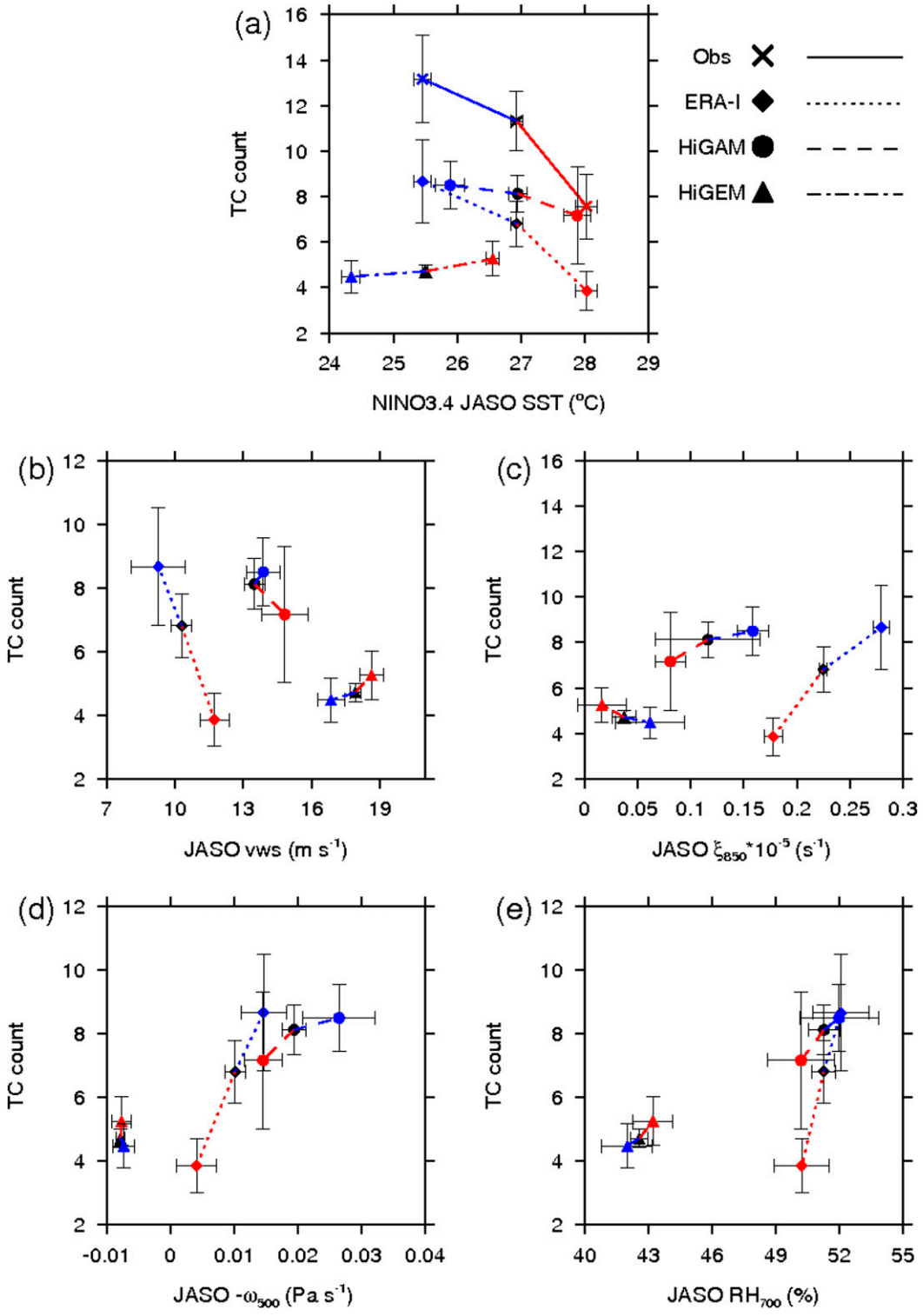

FIG. 9. Scatterplot of tropical cyclone counts vs large-scale environmental parameters for the North Atlantic, averaged over the region 10°–20°N, 275°–340°E during July–October. Red symbols represent the climatology of El Niño years, blue symbols represent the climatology of La Niña years, and black symbols represent the climatology of all years for (a) Niño-3.4 SST anomaly, (b) vertical wind shear, (c) relative vorticity, (d) mean ascent at 500 hPa, and (e) relative humidity at 700 hPa. Observations are shown by the cross, ERA-Interim is shown by diamonds, HiGAM is shown by circles, and HiGEM is shown by triangles. The line styles distinguish between model and observations. The error bars denote the 90% confidence interval.

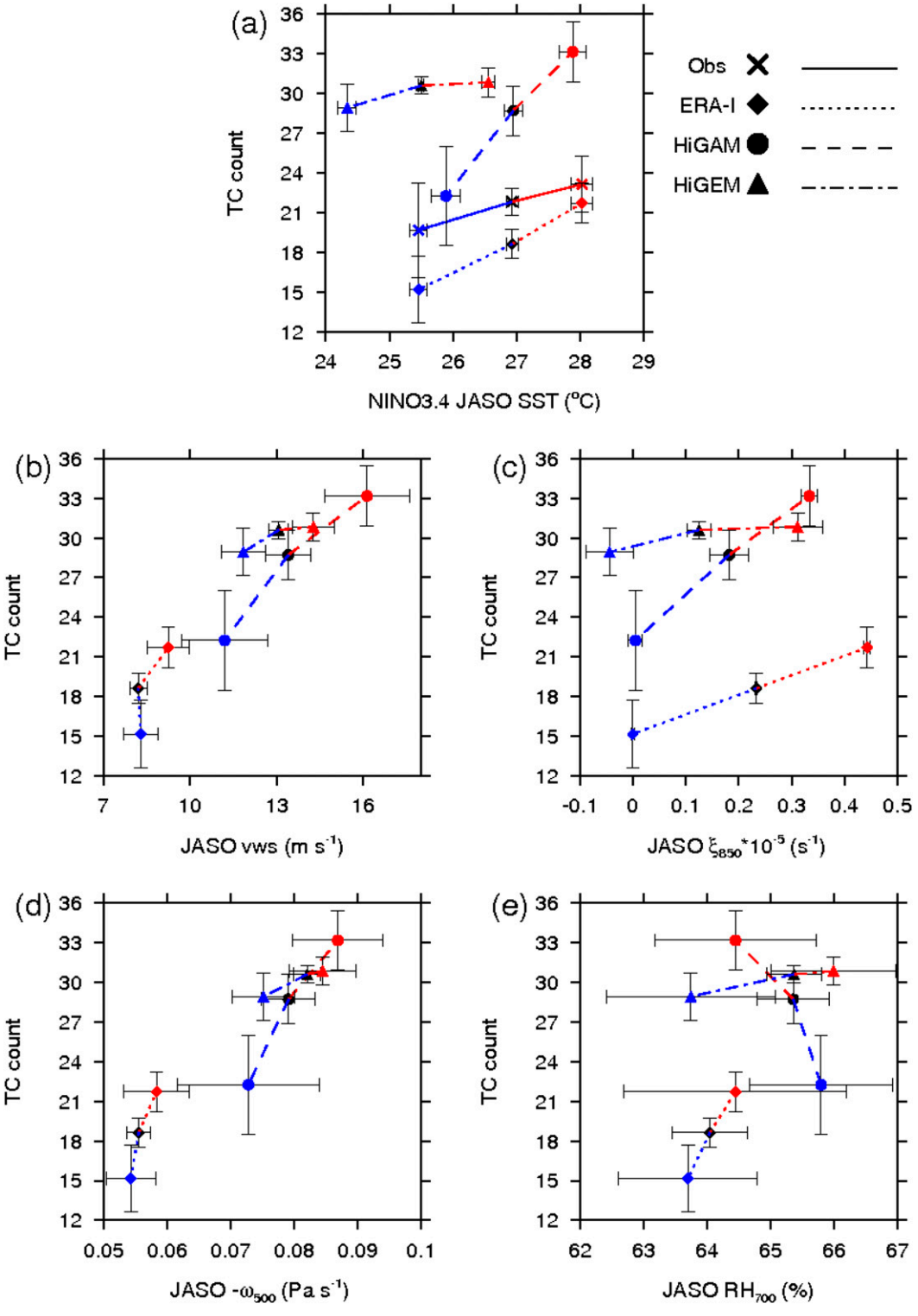

FIG. 10. Scatterplot of tropical cyclone counts vs large-scale environmental parameters for the western North Pacific, averaged over the region 5°–20°N, 130°–170°E during July–October. Red symbols represent the climatology of El Niño years, blue symbols represent the climatology of La Niña years, and black symbols represent the climatology of all years for (a) Niño-3.4 SST anomaly, (b) vertical wind shear, (c) relative vorticity, (d) mean ascent at 500 hPa, and (e) relative humidity at 700 hPa. The error bars denote the 90% confidence interval. Symbols and line styles are as in Fig. 9.

further in Bell et al. (2013), even though vertical wind shear is stronger in HiGAM and HiGEM than in ERA-Interim. In addition, vertical wind shear increases during El Niño years along with an increase in tropical cyclones, indicating that vertical wind shear is not an important driver of tropical cyclone activity over the main development region (Zhao and Held 2012; Strachan et al. 2013). The variability of tropical cyclones with ENSO in this basin arises from the variability in vorticity (Camargo et al. 2007b). HiGAM simulates a large variability of relative vorticity, which causes large variability in the number of tropical cyclones. HiGEM is also able to simulate the relationship of vorticity with ENSO, although the tropical cyclone counts do not respond during El Niño years. Research using track density, as a measurement of spatial tropical cyclone activity, in the region of interest shows an increase of tropical cyclones in HiGEM along with the increase of relative vorticity during El Niño years (not shown). The relative humidity at 700 hPa is slightly larger in the mean state of both HiGAM and HiGEM, which increases the number of tropical cyclones that form each year compared to that observed. The relationship of relative humidity at 700 hPa with ENSO in HiGAM and HiGEM show distinct differences; however, the changes are small and are associated with larger interannual variability. The simulated tropical cyclones in this region are sensitive to a change in mean ascent at 500 hPa. Wang et al. (2013) discussed how environmental factors impact tropical cyclone frequency differently on the interbasin scale in the western North Pacific.

5. Discussion

Simulating the correct spatial SST pattern of ENSO is a necessary but not sufficient requirement for an accurate representation of the global ENSO teleconnections in an AOGCM. Dawson et al. (2013) found an increase in the oceanic resolution produced more accurate ENSO teleconnections compared to an increase in only the atmospheric resolution because of an improvement in the mean-state and ENSO variability. Errors in the atmospheric teleconnections simulated in HiGEM stem from mean-state SST biases and errors in the spatial pattern of ENSO-associated SST. Zhu et al. (2012) found that the simulated mean state of vertical wind shear over the North Atlantic was shown to play a critical role in how the remote influence of ENSO modulates the vertical wind shear. HiGEM has a large mean-state bias of vertical wind shear over the North Atlantic and an underestimation of climatological frequency of tropical cyclones compared to observations (Bell et al. 2013). In addition, HiGEM does not capture the expected tropical cyclone variability associated with El Niño and La Niña events in the North Atlantic. Errors in the variability of ENSO–vertical wind shear teleconnection over the North Atlantic in HiGEM are caused by errors in the spatial pattern of ENSO-associated SST. As the maximum SST warming occurs too far west compared to observations, the eastward atmospheric branch of the Walker circulation does not reach into the North Atlantic. As a result, the coupled model does not capture the dipole of vertical wind shear over the northeast Pacific and North Atlantic. However, the westward extension of ENSO-associated SSTs simulates a realistic ENSO–tropical cyclone teleconnection in the Indian Ocean. The mean state of vertical wind shear over the tropical North Atlantic is reduced in the uncoupled model, HiGAM. There are still errors in the vertical wind shear variability, with slightly more vertical wind shear in La Niña years than the climatology. When the vertical shear is low enough so that it does not dominate the reduction in tropical cyclone signal, the other governing environmental parameters may have a role in influencing tropical cyclone variability, such as the mean ascent at 500 hPa and relative vorticity, which are better captured in HiGAM than in HiGEM.

While the HiGAM simulation shows a marked improvement of the ENSO–tropical cyclone teleconnection in the western North Pacific, there are still some limitations because of inaccurate representation of atmospheric teleconnection processes. As discussed in Shaffrey et al. (2009), HiGEM has a large mean-state precipitation bias over the western North Pacific. The mean-state precipitation bias in HiGEM remains in HiGAM over the western North Pacific. The precipitation is in response to stronger ascent, which likely results in too many tropical cyclones forming (Bell et al. 2013). The variability in terms of tropical cyclone location and the number of tropical cyclones per season is simulated more accurately in HiGAM then in HiGEM. This is attributed here to the greater variability of mean ascent at 500 hPa ($-\omega_{500}$). The atmosphere in HiGAM has a larger source of heat than HiGEM without the presence of air–sea coupled feedbacks. During El Niño years the warmer SST leads to more intense tropical convection. Although this is not entirely clear in the variability of relative humidity shown in Fig. 10, this parameter is associated with large errors bars and is sensitive to the area average used. A basinwide area average shows a similar midlevel relative humidity pattern in HiGAM to that observed (not shown). It may be suggested that the greater variability of tropical cyclone activity in the western North Pacific in HiGAM is influenced by the differences in simulation lengths of HiGEM and HiGAM. However, a 23-yr period with

a similar number of ENSO events as that in HiGAM in HiGEM shows the results remain largely unchanged (not shown).

6. Conclusions

It is important to evaluate the ability of GCMs to simulate realistic ENSO-associated tropical cyclone teleconnections for seasonal forecasting and before predictions are made for tropical cyclones and climate change using GCMs (Mori et al. 2013). The simulated global ENSO–tropical cyclone teleconnection has been investigated with the use of a 150-yr present-day high-resolution AOGCM experiment. The 150-yr present-day HiGEM simulation gives robust statistics of the ENSO–tropical cyclone teleconnection. The relationship was also investigated further using an AGCM forced with observed SSTs.

The coupled model, HiGEM, is able to capture the observed shift in tropical cyclone location with ENSO in the western North Pacific and north Indian Ocean. However, HiGEM is not able to capture the expected tropical cyclone response in the North Atlantic. In terms of large-scale environmental changes with ENSO, the biases in mean ascent at 500 hPa and lack of low-level vorticity variability in the western North Pacific are found to be the limiting factors in capturing the expected magnitude of the ENSO–tropical cyclone teleconnection. The large-scale environment in the North Atlantic is not influenced by ENSO variability in HiGEM. In particular, the vertical wind shear response over the Caribbean is not captured, explaining why the tropical cyclone response is erroneous in that region. The atmosphere-only model, HiGAM, reveals limitations in the coupled model that are due to inaccurate SSTs, as well as shortcomings that remain because of inaccurate representation of atmospheric teleconnection processes. HiGAM simulates the dipole of vertical wind shear in the northeast Pacific and Caribbean Sea, which is not found in HiGEM and therefore the expected tropical cyclone teleconnection. Although the large-scale mean ascent at 500-hPa bias remains in HiGAM over the western North Pacific, the tropical cyclone variability is much better simulated because of a more accurate representation of low-level vorticity with ENSO.

The tropical cyclone changes with climate change found in Bell et al. (2013) are somewhat similar to the El Niño response found in this study. How ENSO will change in the future (Collins et al. 2010) will have a large influence on future tropical cyclone activity. In the near future, ENSO and other modes of natural variability will dominate variability of tropical cyclone activity. It is therefore important that a similar emphasis is placed on understanding the global ENSO–tropical cyclone teleconnection as with tropical cyclones and climate change using GCMs (Mori et al. 2013). Research is currently being undertaken to reduce the coupled biases and improve ENSO-associated teleconnections in the Hadley Centre Climate Model with the use of coupled higher-resolution oceanic (¼°) and atmospheric (25 km) models. An investigation into the change of tropical cyclone intensity in each basin with ENSO would be of use to understand dynamical seasonal forecasts, however we believe this should be left to a higher-resolution atmosphere-only GCM such as in Zhou et al. (2013). The analysis in this paper should be applied to many GCMs to increase the sample size of tropical cyclones and to investigate how well other models simulate the ENSO–tropical cyclone teleconnection (Wang et al. 2014). Further research into the role of ocean coupling on the simulation of the ENSO–tropical cyclone connection using an AGCM prescribed with the simulated SST from an AOGCM would provide further understanding.

Acknowledgments. We thank Nicholas Klingaman for helpful comments. This research was supported by NERC Ph.D. Grant NE/I528569/1 and a collaboration between the University of Reading and Willis. The model described was developed from HadGEM1 by the U.K. High-Resolution Modelling (HiGEM) Project and the U.K. Japan Climate Collaboration (UJCC). UJCC was jointly funded by NERC and by the Joint DECC/Defra Met Office Hadley Centre Climate Programme (GA01101). HiGEM is supported by a NERC High Resolution Climate Modelling Grant (R8/H12/123). Model integrations were performed using the Japanese Earth Simulator supercomputer, supported by JAMSTEC.

REFERENCES

Adler, R. F., and Coauthors, 2003: The Version-2 Global Precipitation Climatology Project (GPCP) monthly precipitation analysis (1979–present). *J. Hydrometeor.,* **4,** 1147–1167, doi:10.1175/1525-7541(2003)004<1147:TVGPCP>2.0.CO;2.

Aiyyer, A. R., and C. Thorncroft, 2006: Climatology of vertical wind shear over the tropical Atlantic. *J. Climate,* **19,** 2969–2983, doi:10.1175/JCLI3685.1.

Alexander, M., I. Bladé, M. Newman, J. R. Lanzante, N.-C. Lau, and J. D. Scott, 2002: The atmospheric bridge: The influence of ENSO teleconnections on air–sea interaction over the global oceans. *J. Climate,* **15,** 2205–2231, doi:10.1175/1520-0442(2002)015<2205:TABTIO>2.0.CO;2.

Bell, R., J. Strachan, P. L. Vidale, K. I. Hodges, and M. Roberts, 2013: Response of tropical cyclones to idealized climate change experiments in a global high-resolution coupled

general circulation model. *J. Climate,* **26,** 7966–7980, doi:10.1175/JCLI-D-12-00749.1.

Bengtsson, L., K. I. Hodges, and M. Esch, 2007: Tropical cyclones in a T159 resolution global climate model: Comparison with observations and re-analysis. *Tellus,* **59A,** 396–416, doi:10.1111/j.1600-0870.2007.00236.x.

Bruyère, C. L., G. J. Holland, and E. Towler, 2012: Investigating the use of a genesis potential index for tropical cyclones in the North Atlantic basin. *J. Climate,* **25,** 8611–8626, doi:10.1175/JCLI-D-11-00619.1.

Camargo, S. J., A. G. Barnston, P. J. Klotzbach, and C. W. Landsea, 2007a: Seasonal tropical cyclone forecasts. *WMO Bull.,* **56,** 297–309.

——, K. A. Emanuel, and A. H. Sobel, 2007b: Use of a genesis potential index to diagnose ENSO effects on tropical cyclone genesis. *J. Climate,* **20,** 4819–4834, doi:10.1175/JCLI4282.1.

Chan, J. C. L., 1985: Tropical cyclone activity in the northwest Pacific in relation to the El Niño/Southern Oscillation phenomenon. *Mon. Wea. Rev.,* **113,** 599–606, doi:10.1175/1520-0493(1985)113<0599:TCAITN>2.0.CO;2.

——, and K. S. Liu, 2004: Global warming and western North Pacific typhoon activity from an observational perspective. *J. Climate,* **17,** 4590–4602, doi:10.1175/3240.1.

Chand, S. S., J. McBride, K. J. Tory, M. C. Wheeler, and K. J. E. Walsh, 2013: Impact of different ENSO regimes on southwest Pacific tropical cyclones. *J. Climate,* **26,** 600–608, doi:10.1175/JCLI-D-12-00114.1.

Chu, P.-S., 2004: ENSO and tropical cyclone activity. *Hurricanes and Typhoons: Past, Present and Future,* R. J. Murname and K.-B. Liu, Eds., Columbia University Press, 297–332.

Collins, M., and Coauthors, 2010: The impact of global warming on the tropical Pacific Ocean and El Niño. *Nat. Geosci.,* **3,** 391–397, doi:10.1038/ngeo868.

Dawson, A., A. Matthews, D. Stevens, M. Roberts, and P.-L. Vidale, 2013: Importance of oceanic resolution and mean state on the extra-tropical response to El Niño in a matrix of coupled models. *Climate Dyn.,* **41** (5–6), 1439–1452, doi:10.1007/s00382-012-1518-6.

Dee, D. P., and Coauthors, 2011: The ERA-Interim reanalysis: Configuration and performance of the data assimilation system. *Quart. J. Roy. Meteor. Soc.,* **137,** 553–597, doi:10.1002/qj.828.

Delworth, T. L., and Coauthors, 2012: Simulated climate and climate change in the GFDL CM2.5 high-resolution coupled climate model. *J. Climate,* **25,** 2755–2781, doi:10.1175/JCLI-D-11-00316.1.

Diamond, H. J., A. M. Lorrey, and J. A. Renwick, 2013: A southwest Pacific tropical cyclone climatology and linkages to the El Niño–Southern Oscillation. *J. Climate,* **26,** 3–25, doi:10.1175/JCLI-D-12-00077.1.

Emanuel, K. A., and D. S. Nolan, 2004: Tropical cyclone activity and the global climate system. *26th Conf. on Hurricanes and Tropical Meteorology,* Miami, FL, Amer. Meteor. Soc., 10A.2 [Available online at https://ams.confex.com/ams/pdfpapers/75463.pdf.]

Felton, C. S., B. Subrahmanyam, and V. S. N. Murty, 2013: ENSO modulated cyclogenesis over the Bay of Bengal. *J. Climate,* **26,** 9806–9818, doi:10.1175/JCLI-D-13-00134.1.

Frank, W. M., and G. S. Young, 2007: The interannual variability of tropical cyclones. *Mon. Wea. Rev.,* **135,** 3587–3598, doi:10.1175/MWR3435.1.

Gill, A. E., 1980: Some simple solutions for heat-induced tropical circulation. *Quart. J. Roy. Meteor. Soc.,* **106,** 447–462, doi:10.1002/qj.49710644905.

Goldenberg, S. B., and L. J. Shapiro, 1996: Physical mechanisms for the association of El Niño and West African rainfall with Atlantic major hurricane activity. *J. Climate,* **9,** 1169–1187, doi:10.1175/1520-0442(1996)009<1169:PMFTAO>2.0.CO;2.

Gray, W. M., 1984: Atlantic seasonal hurricane frequency. Part I: El Niño and 30 mb quasi-biennial oscillation influences. *Mon. Wea. Rev.,* **112,** 1649–1668, doi:10.1175/1520-0493(1984)112<1649:ASHFPI>2.0.CO;2.

——, and J. D. Sheaffer, 1991: El Niño and QBO influences on tropical cyclone activity. *Teleconnections Linking Worldwide Anomalies,* M. H. Glantz, R. W. Katz, and N. Nicholls, Eds., Cambridge University Press, 257–284.

Guilyardi, E., A. Wittenberg, A. Fedorov, M. Collins, C. Wang, A. Capotondi, G. J. van Oldenborgh, and T. Stockdale, 2009: Understanding El Niño in ocean–atmosphere general circulation models: Progress and challenges. *Bull. Amer. Meteor. Soc.,* **90,** 325–340, doi:10.1175/2008BAMS2387.1.

Iizuka, S., and T. Matsuura, 2008: ENSO and western North Pacific tropical cyclone activity simulated in a CGCM. *Climate Dyn.,* **30** (7–8), 815–830, doi:10.1007/s00382-007-0326-x.

——, and ——, 2009: Relationship between ENSO and North Atlantic tropical cyclone frequency simulated in a coupled general circulation model. *Hurricanes and Climate Change,* J. B. Elsner and T. H. Jagger, Eds., Springer, 323–338.

Johns, T. C., and Coauthors, 2006: The new Hadley Centre climate model (HadGEM1): Evaluation of coupled simulations. *J. Climate,* **19,** 1327–1353, doi:10.1175/JCLI3712.1.

Kalnay, E., and Coauthors, 1996: The NCEP/NCAR 40-Year Reanalysis Project. *Bull. Amer. Meteor. Soc.,* **77,** 437–471, doi:10.1175/1520-0477(1996)077<0437:TNYRP>2.0.CO;2.

Kim, H.-M., P. J. Webster, and J. A. Curry, 2009: Impact of shifting patterns of Pacific Ocean warming on North Atlantic tropical cyclones. *Science,* **325,** 77–80, doi:10.1126/science.1174062.

Klotzbach, P. J., 2011: El Niño–Southern Oscillation's impact on Atlantic basin hurricanes and U.S. landfalls. *J. Climate,* **24,** 1252–1263, doi:10.1175/2010JCLI3799.1.

Knapp, K. R., M. C. Kruk, D. H. Levinson, H. J. Diamond, and C. J. Neumann, 2010: The International Best Track Archive for Climate Stewardship (IBTrACS): Unifying tropical cyclone data. *Bull. Amer. Meteor. Soc.,* **91,** 363–376, doi:10.1175/2009BAMS2755.1.

Kossin, J. P., S. J. Camargo, and M. Sitkowski, 2010: Climate modulation of North Atlantic hurricane tracks. *J. Climate,* **23,** 3057–3076, doi:10.1175/2010JCLI3497.1.

Kuleshov, Y., L. Qi, R. Fawcett, and D. Jones, 2008: On tropical cyclone activity in the Southern Hemisphere: Trends and the ENSO connection. *Geophys. Res. Lett.,* **35,** L14S08, doi:10.1029/2007GL032983.

Landsea, C. W., and J. L. Franklin, 2013: Atlantic hurricane database uncertainty and presentation of a new database format. *Mon. Wea. Rev.,* **141,** 3576–3592, doi:10.1175/MWR-D-12-00254.1.

Langenbrunner, B., and J. D. Neelin, 2013: Analyzing ENSO teleconnections in CMIP models as a measure of model fidelity in simulating precipitation. *J. Climate,* **26,** 4431–4446, doi:10.1175/JCLI-D-12-00542.1.

Manganello, J. V., and Coauthors, 2012: Tropical cyclone climatology in a 10-km global atmospheric GCM: Toward weather-resolving climate modeling. *J. Climate,* **25,** 3867–3893, doi:10.1175/JCLI-D-11-00346.1.

Maue, R. N., 2009: Northern Hemisphere tropical cyclone activity. *Geophys. Res. Lett.,* **36,** L05805, doi:10.1029/2008GL035946.

McGauley, M. G., and D. S. Nolan, 2011: Measuring environmental favorability for tropical cyclogenesis by statistical analysis of threshold parameters. *J. Climate,* **24,** 5968–5997, doi:10.1175/2011JCLI4176.1.

Mori, M., and Coauthors, 2013: Hindcast prediction and near-future projection of tropical cyclone activity over the western North Pacific using CMIP5 near-term experiments with MIROC. *J. Meteor. Soc. Japan,* **91,** 431–452, doi:10.2151/jmsj.2013-402.

Murakami, H., and M. Sugi, 2010: Effect of model resolution on tropical cyclone climate projections. *SOLA,* **6,** 73–76, doi:10.2151/sola.2010-019.

——, and B. Wang, 2010: Future change of North Atlantic tropical cyclone tracks: Projection by a 20-km-mesh global atmospheric model. *J. Climate,* **23,** 2699–2721, doi:10.1175/2010JCLI3338.1.

——, and Coauthors, 2012: Future changes in tropical cyclone activity projected by the new high-resolution MRI-AGCM. *J. Climate,* **25,** 3237–3260, doi:10.1175/JCLI-D-11-00415.1.

Nicholls, N., 1979: A possible method for predicting seasonal tropical cyclone activity in the Australian region. *Mon. Wea. Rev.,* **107,** 1221–1224, doi:10.1175/1520-0493(1979)107<1221:APMFPS>2.0.CO;2.

Rayner, N. A., D. E. Parker, E. B. Horton, C. K. Folland, L. V. Alexander, D. P. Rowell, E. C. Kent, and A. Kaplan, 2003: Global analyses of sea surface temperature, sea ice, and night marine air temperature since the late nineteenth century. *J. Geophys. Res.,* **108,** 4407, doi:10.1029/2002JD002670.

Ringer, M. A., and Coauthors, 2006: The physical properties of the atmosphere in the new Hadley Centre Global Environmental Model (HadGEM1). Part II: Aspects of variability and regional climate. *J. Climate,* **19,** 1302–1326, doi:10.1175/JCLI3713.1.

Roberts, M. J., and Coauthors, 2009: Impact of resolution on the tropical Pacific circulation in a matrix of coupled models. *J. Climate,* **22,** 2541–2556, doi:10.1175/2008JCLI2537.1.

Shaffrey, L. C., and Coauthors, 2009: U.K. HiGEM: The new U.K. high-resolution global environment model—Model description and basic evaluation. *J. Climate,* **22,** 1861–1896, doi:10.1175/2008JCLI2508.1.

Shaman, J., and E. D. Maloney, 2012: Shortcomings in climate model simulations of the ENSO-Atlantic hurricane teleconnection. *Climate Dyn.,* **38,** 1973–1988, doi:10.1007/s00382-011-1075-4.

——, S. K. Esbensen, and E. D. Maloney, 2009: The dynamics of the ENSO–Atlantic hurricane teleconnection: ENSO-related changes to the North African–Asian jet affect Atlantic basin tropical cyclogenesis. *J. Climate,* **22,** 2458–2482, doi:10.1175/2008JCLI2360.1.

Smith, D. M., R. Eade, N. J. Dunstone, D. Fereday, J. M. Murphy, H. Pohlmann, and A. A. Scaife, 2010: Skilful multi-year predictions of Atlantic hurricane frequency. *Nat. Geosci.,* **3,** 846–849, doi:10.1038/ngeo1004.

Smith, T. M., P. A. Arkin, J. J. Bates, and G. J. Huffman, 2006: Estimating bias of satellite-based precipitation estimates. *J. Hydrometeor.,* **7,** 841–856, doi:10.1175/JHM524.1.

Solomon, A., and M. Newman, 2012: Reconciling disparate twentieth-century Indo-Pacific ocean temperature trends in the instrumental record. *Nat. Climate Change,* **2,** 691–699.

Spencer, H., and J. M. Slingo, 2003: The simulation of peak and delayed ENSO teleconnections. *J. Climate,* **16,** 1757–1774, doi:10.1175/1520-0442(2003)016<1757:TSOPAD>2.0.CO;2.

Strachan, J., P. L. Vidale, K. Hodges, M. Roberts, and M.-E. Demory, 2013: Investigating global tropical cyclone activity with a hierarchy of AGCMs: The role of model resolution. *J. Climate,* **26,** 133–152, doi:10.1175/JCLI-D-12-00012.1.

Taylor, K., D. Williamson, and F. W. Zwiers, 2000: The sea surface temperature and sea-ice boundary conditions for AMIPII simulations. PCMDI Tech. Rep., 66 pp.

Tippett, M. K., S. J. Camargo, and A. H. Sobel, 2011: A Poisson regression index for tropical cyclone genesis and the role of large-scale vorticity in genesis. *J. Climate,* **24,** 2335–2357, doi:10.1175/2010JCLI3811.1.

Vitart, F., and J. L. Anderson, 2001: Sensitivity of Atlantic tropical storm frequency to ENSO and interdecadal variability of SSTs in an ensemble of AGCM integrations. *J. Climate,* **14,** 533–545, doi:10.1175/1520-0442(2001)014<0533:SOATSF>2.0.CO;2.

Wang, B., and J. C. L. Chan, 2002: How strong ENSO events affect tropical storm activity over the western North Pacific. *J. Climate,* **15,** 1643–1658, doi:10.1175/1520-0442(2002)015<1643:HSEEAT>2.0.CO;2.

Wang, C., 2002: Atlantic climate variability and its associated atmospheric circulation cells. *J. Climate,* **15,** 1516–1536, doi:10.1175/1520-0442(2002)015<1516:ACVAIA>2.0.CO;2.

——, C. Li, M. Mu, and W. Duan, 2013: Seasonal modulations of different impacts of two types of ENSO events on tropical cyclone activity in the western North Pacific. *Climate Dyn.,* **40** (11–12), 2887–2902, doi:10.1007/s00382-012-1434-9.

Wang, H., and Coauthors, 2014: How well do climate models simulate the variability of Atlantic tropical cyclones associated with ENSO? *J. Climate,* in press.

Wolter, K., and M. S. Timlin, 2011: El Niño/Southern Oscillation behaviour since 1871 as diagnosed in an extended multivariate ENSO index. *Int. J. Climatol.,* **31,** 1074–1087, doi:10.1002/joc.2336.

Wu, G., and N.-C. Lau, 1992: A GCM simulation of the relationship between tropical-storm formation and ENSO. *Mon. Wea. Rev.,* **120,** 958–977, doi:10.1175/1520-0493(1992)120<0958:AGSOTR>2.0.CO;2.

Zhao, M., and I. M. Held, 2012: TC-permitting GCM simulations of hurricane frequency response to sea surface temperature anomalies projected for the late-twenty-first century. *J. Climate,* **25,** 2995–3009, doi:10.1175/JCLI-D-11-00313.1.

——, ——, S. J. Lin, and G. A. Vecchi, 2009: Simulations of global hurricane climatology, interannual variability, and response to global warming using a 50-km resolution GCM. *J. Climate,* **22,** 6653–6678, doi:10.1175/2009JCLI3049.1.

Zhou, Y., J. Jiang, Y. Lu, and A. Huang, 2013: Revealing the effects of the El Niño-Southern Oscillation on tropical cyclone intensity over the western North Pacific from a model sensitivity study. *Adv. Atmos. Sci.,* **30,** 1117–1128, doi:10.1007/s00376-012-2109-5.

Zhu, X., R. Saravanan, and P. Chang, 2012: Influence of mean flow on the ENSO–vertical wind shear relationship over the northern tropical Atlantic. *J. Climate,* **25,** 858–864, doi:10.1175/JCLI-D-11-00213.1.